Physics of Fluids

RESEARCH ARTICLE | JULY 26 2024

Spinning dynamics of self-excited azimuthal acoustic modes in cavities

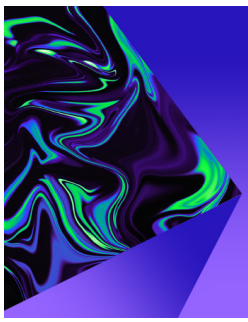
Mahmoud Shaaban ; Rasha Noufal ; Mohammed Alziadeh; Atef Mohany

Check for updates

Physics of Fluids 36, 075197 (2024)
https://doi.org/10.1063/5.0215571

View Online
Export Citation

26 July 2024 14:04:15


Physics of Fluids
Special Topic:
Selected Papers from the 2023 Non-Newtonian Fluid Mechanics Symposium in China
Submit Today
AIP Publishing

AIP Publishing

Physics of Fluids ARTICLE pubs.aip.org/aip/pof

Spinning dynamics of self-excited azimuthal acoustic modes in cavities

Cite as: Phys. Fluids **36**, 075197 (2024); doi: 10.1063/5.0215571
Submitted: 24 April 2024 · Accepted: 10 July 2024 ·
Published Online: 26 July 2024

View Online Export Citation CrossMark

Mahmoud Shaaban,[1,2] Rasha Noufal,[1] Mohammed Alziadeh,[1] and Atef Mohany[1,a)]

AFFILIATIONS

[1]Fluid-Structure Interaction and Noise Control Laboratory, Ontario Tech University, Oshawa, Ontario L1H 7K4, Canada
[2]School of Engineering and Applied Sciences, Nile University, Giza, Egypt

[a)]Author to whom correspondence should be addressed: atef.mohany@ontariotechu.ca

ABSTRACT

The coupling between the shear layer separating between axisymmetric leading and trailing edges and the azimuthal modes of a cavity may result in self-excited spinning acoustic resonance. Notably, the spinning direction remains one of the less understood features of the coupled mode dynamics. In this work, compressible large eddy simulation is used to model the excitation of azimuthal acoustic modes in rectangular cavities. To verify the effect of aspect ratio on the resonant acoustic mode excitation, three cavities with aspect ratios $W/H = 1.0$, 0.95, and 0.90 are considered, all with the same shear layer length. While the square cross section cavity excited a pure spinning mode similar to that for a circular cavity, a small deviation from the square geometry in the coupled acoustic-flow fields leads to an attenuation of the acoustic mode amplitude. This attenuation results from a change in the phase characteristics, which impacts the spinning mode behavior. A slight side length mismatch drives a frequency difference between the two superimposed degenerate modes, resulting in a periodic reversal of the spinning direction. As the mismatch increases, the shear layer fails to excite one of the two modes, leading to the dominance of the other, and the aeroacoustic mode becomes fully stationary. More importantly, the shear layer follows the acoustic mode behavior such that the separation point changes its spinning direction accordingly. Consequently, the shape of the shear layer changes over time, resembling a clockwise helix, a counterclockwise helix, or crescent pairs closely following the acoustic mode.

Published under an exclusive license by AIP Publishing. https://doi.org/10.1063/5.0215571

26 July 2024 14:04:15

I. INTRODUCTION

Self-excited acoustic resonance over cavities is a significant concern in many engineering applications, such as pipelines, boilers, side branches, and other applications.[1–6] Grazing flow leaving the leading edge of a cavity creates a shear layer that may become unstable and oscillate across the cavity mouth plane. In many configurations, the leading and trailing edges are opposite axisymmetric circles such that oscillations tend to occur in the cylindrical plane surrounding the free flow inside the cavity. This flow can be observed in applications such as combustion chambers, valve gates, and turbomachinery.[7–9] If the oscillation frequency coincides with any of the acoustic mode frequencies of the enclosure, a fluid-resonant feedback mechanism is initiated.[10] The energy transfer sustained by the fluid-resonant feedback mechanism amplifies the flow instabilities, resulting in severe noise and vibration.[11–13] This phenomenon is known as flow-excited acoustic resonance. The onset of flow-excited acoustic resonance is a serious design concern, since the increased noise and vibration levels lead to a degradation in the safety and reliability of equipment as well as potential economic losses due to component failures and unscheduled equipment maintenance.

Modeling the complex nature of the energy exchange process in a rectangular cavity with axisymmetric leading and trailing edges represents a challenge. Due to the symmetry of the shear layer separation plane around the free stream axis, three primary acoustic mode orientations can occur in the cavity volume. As shown in Fig. 1, the fundamental orientations are longitudinal, diametral, and azimuthal modes. Each one of these modes exhibits unique patterns of acoustic energy distribution and propagation.[4] Longitudinal acoustic modes are oriented in the flow direction and can propagate into the upstream and downstream ducts and, thus, do not interfere with the shear layer oscillations. Diametral acoustic modes have polar symmetry around the flow axis, and while they can be excited by the shear layer oscillations, there is no possibility for spinning. Azimuthal modes have pressure nodes and antinodes around the outer perimeter of the cavity, and a pressure antinodal plane always passes by the center, such that it can be excited by the shear layer oscillations. Because the cutoff frequency of transverse modes inside the larger cavity is lower than that in the upstream and downstream flow ducts, transverse modes excited in the cavity remain primarily trapped within the cavity with negligible acoustic radiation losses.[14] The shear layer traveling across the plane

Published under an exclusive license by AIP Publishing

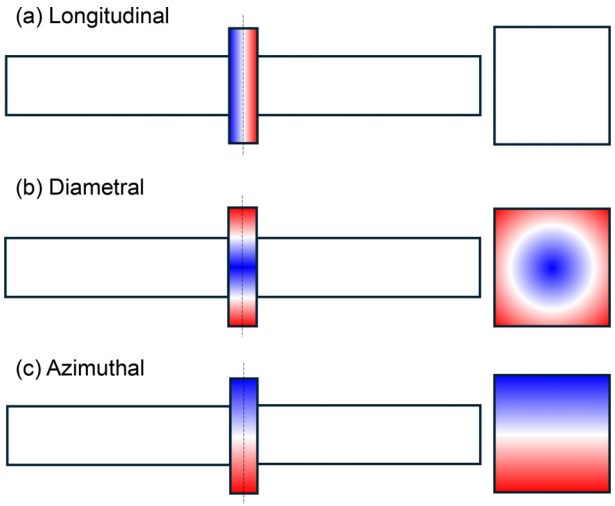


FIG. 1. Fundamental mode orientations in a rectangular cavity with opposite axisymmetric leading and trailing edges: (a) fundamental longitudinal mode, (b) fundamental diametral mode, and (c) fundamental azimuthal mode.

impinges on the trailing edge, creating fluctuations at a regular frequency that depends on the flow velocity and geometry.[15] At certain flow velocities, the pressure oscillations can coincide with an acoustic mode frequency, which may then influence the shear layer behavior, leading to the excitation of severe acoustic resonance. Azimuthal acoustic modes pose a challenge to the design of gas turbine combustors.[16,17] Modern combustors designed to significantly reduce emissions through lean premixed combustion are particularly vulnerable to azimuthal oscillations and typically experience vibrations that may result in structural damage.[18]

In two opposite rectangular cavities with finite leading edges, Abdelmwgoud *et al.*[5] reported only the excitation of stationary transverse and longitudinal modes. On the other hand, the configuration of a cavity with opposite axisymmetric leading and trailing edges gives rise to the excitation of stationary or spinning azimuthal acoustic modes. The occurrence of azimuthal acoustic modes in a cylindrical waveguide was first observed experimentally by Parker[19] and formulated analytically by Evans *et al.*[20] Subsequently, many studies have been performed to understand the nature of the azimuthal acoustic modes in different configurations. Parker[21,22] suggested that the geometry of thin cavities connected to a smaller duct at both ends gives rise to conditions where azimuthal acoustic modes may become confined or trapped within the cavity, leading to sustained resonance. Awny and Ziada[23] experimentally reported the self-excitation of azimuthal acoustic modes by flow in an axisymmetric circular cavity connected to a duct. Hein *et al.*[24] numerically modeled an axisymmetric cavity, showing the self-excitation of trapped acoustic modes. The excited modes are characterized by antisymmetric pressure fluctuations that can spin without any favored azimuthal direction. Additionally, this acoustic mode is essentially "trapped" in the cavity volume and cannot propagate along the duct.

Keller and Escudier[11] observed that stationary azimuthal acoustic modes excited in a cavity connected to a duct may have an arbitrary orientation and attributed this behavior to irregularities in the axisymmetric arrangement. Aly and Ziada[14] carried out a series of experimental studies of axisymmetric shallow cavities to examine the influence of the cavity geometry on the acoustic response to upstream flow. They reported that the flow within a duct could excite different azimuthal acoustic modes, with the modes of higher frequencies excited at higher flow velocities. Aly and Ziada[25] identified three distinct pressure patterns for the excited modes: stationary, partially spinning, or purely spinning, based on the temporal development of the acoustic pressure antinode location in the azimuthal direction. They illustrated that if the cavity geometry is symmetric, the pressure antinodes lacks a fixed point for the pressure antinode along the cavity's circumference.[26] In this case, the generated azimuthal acoustic modes had no preferable azimuthal orientation and may spin within the cavity configuration. However, minor variations in symmetry combined with acoustic damping in the cavity may lead to a preference in orientation, which, in turn, causes a tendency toward a partial spinning behavior.

Ziada *et al.*[27] investigated the excitation of azimuthal acoustic modes in non-axisymmetric cavities such as square and rectangular shapes and, notably, reported the excitation of both stationary and spinning acoustic modes. Contrary to a circular cavity, rectangular and square cavities have preferential azimuthal orientations, which may affect the azimuthal behavior of acoustic modes. They attributed the occurrence of spinning modes to the superposition of two orthogonal modes. Shaaban and Ziada[28] experimentally investigated the flow dynamics over a rectangular cavity, showing that acoustic resonance has a considerable impact on the shear layer dynamics over the rectangular cavity. During the excitation of the longitudinal modes, the strong acoustic oscillations synchronize and strengthen vortex shedding at the leading edge of the rectangular cavity, effectively creating a sound source over the cavity mouth. Wang and Liu[29,30] and Abdelmwgoud *et al.*[4] performed a large eddy simulation (LES) to study the flow and acoustic characteristics of the periodic flow modes and their interaction with oscillation cycles. They noted a significant influence of azimuthal acoustic mode excitation on the structure of the separated shear layer on the leading edge of an axisymmetric cavity. However, their results did not explain the spinning direction and did not report any reversal in the spinning direction similar to that observed in the experiments of Aly and Ziada.[25] In a rectangular cavity connected to a circular waveguide, the azimuthal acoustic mode is expected to interact with the separating shear layer in a nonuniform manner. As the whole shear layer around the circumference of a duct will not be equally excited, the interacting fields exhibit a complex three-dimensional structure, making it challenging to investigate using experimental methods suitable for planar or axisymmetric configurations.[28] Consequently, no details of the effect of spinning azimuthal mode excitation on the shear layer in a rectangular cavity are yet available in the literature.

The spinning direction of the excited acoustic mode is one of the less understood features of the dynamics of the cavity modes excited by the unstable shear layer between opposite axisymmetric leading and trailing edges. In an experimental study, Aly and Ziada[25] noted that in a circular cavity with no preference toward a particular direction, the azimuthal phase in the shear layer is controlled by the acoustic perturbation as the acoustic mode spins. Interestingly, a change in the phase sign was frequently reported, indicating a reversal in the direction of the azimuthal spinning. Ziada *et al.*[27] noticed that the acoustic mode preferred to spin in the counterclockwise direction, and reported that

26 July 2024 14:04:15

Published under an exclusive license by AIP Publishing

some reversal in the direction of spinning did occur. More recently, Faure-Beaulieu *et al.*[31] investigated the influence of coherent fluctuations of the vorticity at the cavity's opening on one of its spinning azimuthal or stationary radial acoustic modes. They examined the coupling between the flow field and the fundamental azimuthal mode as a consequence of the rotational symmetry of the cavity configuration. Faure-Beaulieu *et al.*[32] highlighted three mechanisms that may contribute to a statistical tendency toward a particular spinning mode. First, a difference in stability of the two degenerate modes due to a mean flow swirl may result in the encouragement of acoustic mode spinning. Second, the spinning direction may be determined by the asymmetries of the cavity. Third, an emerging turbulent swirl can engage in feedback with the acoustic mode. While these mechanisms may address the preference for spinning in a particular way, they do not account for a regular reversal of the spinning direction.

In this study, an additional mechanism that contributes to the coupling dynamics of the flow and acoustic modes is illustrated. It was observed that under certain conditions, the mismatch in frequencies between two degenerate modes in the cavity may result in a cyclic reversal of the spinning direction. The two frequencies of the two degenerate azimuthal modes are precisely controlled by modeling a cavity with a rectangular cross section rather than a circular or elliptical cross section. A three-dimensional, compressible LES model is developed to capture the complex coupling between the shear layer dynamics and acoustic mode in a cavity with a rectangular cross section. The width-to-height (W/H) aspect ratio of the rectangular cavities considered in this study is $W/H = 1$ (square), $W/H = 0.95$, and $W/H = 0.90$. The acoustic pressure and the shear layer patterns examined at the aforementioned aspect ratios drive significantly different azimuthal patterns.

II. METHODOLOGY

In this study, the influence of self-excited diametral acoustic modes on the flow dynamics within a three-dimensional cavity volume is investigated using a compressible LES model.

The interaction of the fluid flow and acoustic oscillations is modeled by the compressible Navier–Stokes equations, which model the conservation of mass, momentum, and energy, along with the ideal gas equation of state. The flow velocity vector $\boldsymbol{u}$ satisfies the mass conservation equation:

$$\frac{\partial \rho}{\partial t} + \nabla \cdot (\rho \boldsymbol{u}) = 0. \tag{1}$$

The momentum equation states that

$$\frac{\partial \rho \boldsymbol{u}}{\partial t} + \nabla \cdot (\rho \boldsymbol{u}\boldsymbol{u}) = -\nabla p + \rho \boldsymbol{g} + \frac{\partial}{\partial x_j}\left[\mu\left(\frac{\partial u_i}{\partial x_j} + \frac{\partial u_j}{\partial x_i}\right) - \frac{2}{3}\mu\delta_{ij}\nabla \cdot \boldsymbol{u}\right]. \tag{2}$$

The conservation of the total energy is formulated as

$$\frac{\partial \rho e}{\partial t} + \nabla \cdot (\rho \boldsymbol{u} e) = -\nabla \cdot k\nabla T - p(\nabla \cdot \boldsymbol{u}) + \tau_{ij} \cdot (\nabla \cdot \boldsymbol{u}) + S_e. \tag{3}$$

Figure 2 presents the layout of the numerical domain, which consists of a thin rectangular cavity connected at its upstream and downstream sides to two cylindrical pipes with a diameter of 150 mm. Three different rectangular cavity aspect ratios W/H are considered as shown in Fig. 2. The three aspect ratios are chosen to result in a frequency mismatch for the fundamental acoustic modes of the cavity equal to 0%, 5%, and 10% for $W/H = 1.0$, 0.95, and 0.90, respectively. The leading and trailing edges are opposite circles with centers coincident with the centers of the two rectangular sides.

The dimensions and configuration of the computational domain have been selected to align with the experimental work of Ziada *et al.*[27] to establish a basis for validation. The cylindrical pipe extends 3 pipe diameters (D) (i.e., $3D$) from the cavity in the outlet direction and $2.5D$ toward the inlet direction. These lengths were selected to reduce the impact of the inlet and outlet boundary conditions on the cavity region and mitigate the effect of acoustic radiation from the ends of the numerical model. The difference in distances L_{up} and L_{down} mitigates the potential for a longitudinal acoustic mode excitation with a pressure antinode within the rectangular section.

Eight pressure monitor probes (P_1–P_8), depicted in Fig. 2, are located on the cavity wall at eight equally spaced azimuth angles to record the amplitude and phase characteristics of the induced resonance. These probes are placed around the cavity's perimeter to verify the maximum acoustic pressure amplitude, phase distribution, and spinning behavior of each excited mode. Each time step, the static pressure value is recorded at all probe locations. The numerical model is run for a total flow time of 1 s, which is sufficient for the statistical acoustic and flow quantities to stabilize. The recorded pressure values at each probe location are then processed as a time series. A spectral analysis is used to analyze the dominant frequencies at a resolution of 1 Hz. The acoustic pressure at each probe location is calculated through the root mean square (rms) of the static pressure values recorded after the statistical acoustic pressure values stabilize.

A fully coupled transient solver for compressible Navier–Stokes equations was implemented based on the open source OpenFOAM computational fluid dynamics library. The solver used the PIMPLE algorithm, which is a layered combination of the pressure implicit with splitting of operator (PISO) and semi-implicit method for pressure-linked equations (SIMPLE) algorithms, to resolve the pressure–velocity coupling in a finite volume grid. The properties of air at standard pressure and temperature were used, such that air kinematic viscosity $\nu = 1.5 \times 10^{-5}$ m^2/s, specific heat $c_p = 999$ J/(kg K), and Prandtl number $Pr = 0.7$.

The density, ρ, and internal energy, e, of air were calculated through the ideal gas equation of state. The turbulence in the subgrid scale was modeled by solving a transport equation for the subgrid scale kinetic energy k_{sgs} equation, which is calculated according to the Smagorinsky–Lilly model.[33] The spectral characteristics of the flow velocity are in a good agreement with the predicted turbulence energy decrease over the frequency range of interest. The second order implicit backward Euler scheme was used for temporal discretization. Convective terms in the momentum equation are discretized through a Gauss linear-Upwind scheme, while diffusive terms were discretized by Gauss linear gradient differentiation to ensure second order accuracy.[34] The iterative algorithm continues until a statistically steady oscillating behavior is observed for sufficient time to enable the calculation of the spectral characteristics of forces and fluid quantities in the computational domain.[35]

The computational domain was resolved to a hexahedral grid comprising approximately 9×10^6 node elements to effectively capture the flow dynamics. Figure 3 demonstrates the details of the mesh

26 July 2024 14:04:15

Published under an exclusive license by AIP Publishing

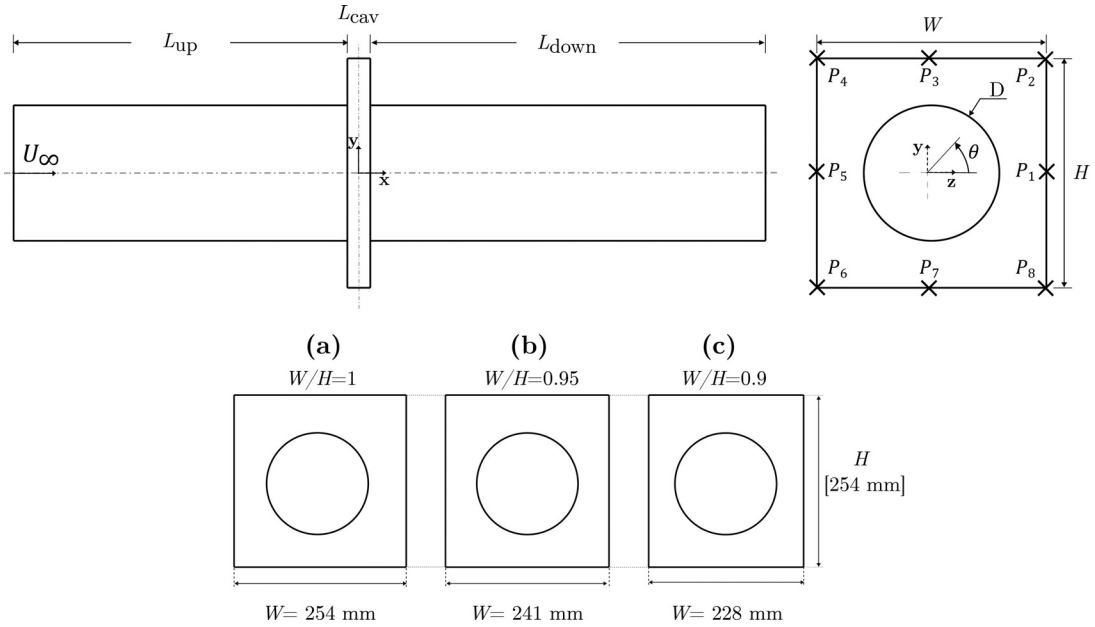


FIG. 2. Layout of the three-dimensional fluid domain and the dimensions of the investigated cavities: (a) square cavity ($W/H = 1.0$), (b) rectangular cavity ($W/H = 0.95$), and (c) rectangular cavity ($W/H = 0.90$).

at a section passing by the middle of the cavity and near the cavity edge. The size of the elements within the grid was selected to maintain an acoustic Courant number under 4.0, such that both the flow and acoustic Courant numbers are sufficiently low to resolve the compressible Navier–Stokes equations and the propagation of sound waves.

The geometric agglomerated algebraic multigrid preconditioned solver (GAMG) was utilized to solve the asymmetric pressure matrix, whereas the preconditioned bi-conjugate gradient solver (PBiCGStab) was used to solve the symmetric matrix parameters including velocity, turbulence kinetic energy, and the specific turbulence dissipation rate. Boundary conditions imposed on the numerical domain were based

26 July 2024 14:04:15

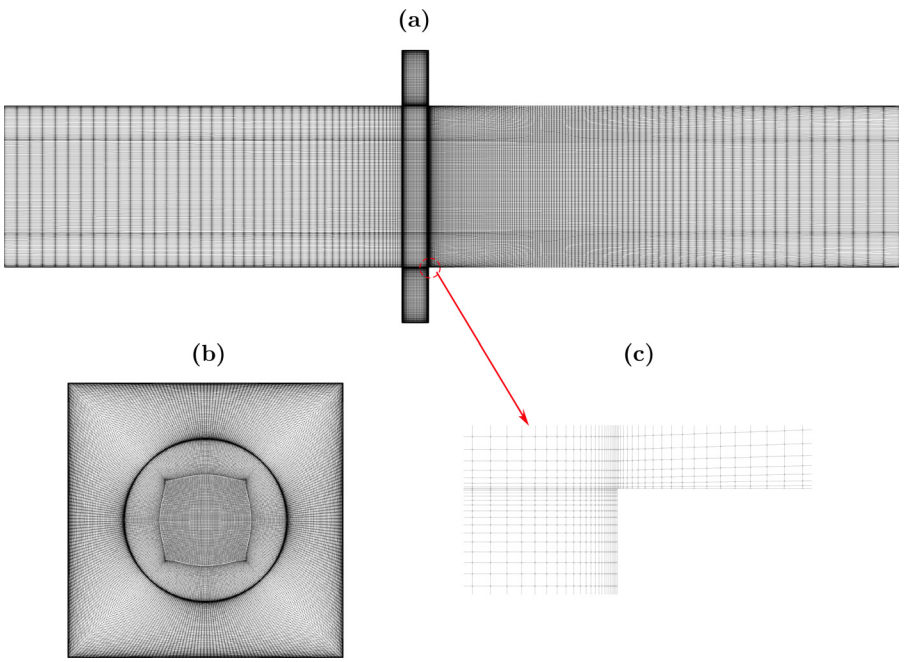


FIG. 3. The computational grid (a) side section, (b) front section at the middle of the cavity, and (c) details of the grid near the cavity edge.

Published under an exclusive license by AIP Publishing

on the experimental conditions of Ziada *et al.*[27] A uniform velocity is set at the inlet boundaries, while the outflow boundaries utilize a zero pressure gradient condition. All internal walls of the cavity are configured with no-slip boundary conditions. The pressure at both the inlet and outlet boundaries is handled using a wave-transmissive condition to prevent reflection. Additionally, the flow near the walls is modeled using a wall function to bridge the gap between the resolved large scales of turbulence in the core flow and the unresolved small scales near the wall.

To verify the accuracy of the LES model used in this study, a grid sensitivity analysis was carried out. Figure 4 illustrates the impact of varying the number of grid elements and time step size on the predicted rms acoustic pressure and the dominant frequency. In Fig. 4(a), the rms acoustic pressure is normalized by the values obtained with the largest grid size, while in Fig. 4(c), it is normalized by the values obtained with the smallest time step. Similarly, the dominant frequency is normalized by the values obtained with the largest grid size in Fig. 4(b) and with the smallest time step in Fig. 4(d). The sensitivity analysis shows that the acoustic pressure and frequency are not significantly altered by changes in the time step and grid size. The invariability of the acoustic pressure and frequency demonstrates the independence of the present simulation results with the mesh and time step. Although the results converge at 6×10^6 nodes, simulations were carried out at 9×10^6 nodes to achieve the required Courant number at the converged time step of 2 μs, ensuring the model's capability to capture the interaction between the flow and sound fields during the excitation of the azimuthal acoustic mode.

The flow velocity at the inlet of the domain was set to closely match the experimental value that resulted in flow-excited acoustic resonance in the work of Ziada *et al.*,[27] to enable validation in terms of the peak acoustic pressure amplitudes. The inlet flow velocity was set as 50 m/s for the square cavity ($W/H=1$). For aspect ratios $W/H=0.95$ and 0.90, two inlet flow velocities were studied to identify the flow velocity at which the higher acoustic pressure occurred. Figure 5 provides a comparison of the normalized rms acoustic pressure, p^*, and frequency, f_a, obtained from the present simulation with the experimental results of Ziada *et al.*[27] for the different cavity aspect ratio W/H. The rms acoustic pressure was normalized with respect to the inlet dynamic pressure, as defined in the following equation:

$$p^* = \frac{2P_{rms}}{\rho_0 U_\infty^2}. \tag{4}$$

As illustrated in Fig. 5, the numerical predictions produced by the simulation are in good agreement with the experimental results of Ziada *et al.*[27] At the flow velocity that results in the maximum acoustic pressure amplitude on the cavity wall, a good agreement is obtained with an error margin of about 1% for f_a and a maximum of 10% for p^*. This shows that the model effectively captures the excitation mechanism of the azimuthal acoustic mode.

To verify that the upstream pipe length is sufficient to ensure the boundary layer thickness is thin compared to the pipe diameter, the mean velocity profile at a flow velocity of 50 m/s for the case of the square cavity ($W/H=1$) is illustrated in Fig. 6. This profile is compared with Laser Doppler Velocimetry (LDV) measurements from Bolduc and Ziada's experiments for the same cavity geometry.[36] The flow velocity profile agrees very well with Bolduc and Ziada's results, indicating that the approach flow velocity profile in the LES simulation closely matches their experiments, with a boundary layer thickness of less than 10 mm.

To verify the nature of degenerate azimuthal modes and the spinning behavior that results from their superposition with or without a frequency mismatch, analytical representation of the two-dimensional cavity modes is calculated.

Given that acoustic waves within a cavity exhibit variation and propagate in the azimuths direction, the quaternion projection, as introduced by Ghirardo and Bothien,[37] emerges as an effective method to characterize the dynamics of the acoustic pressure oscillations. The utilization of quaternion projection enables the precise description of acoustic pressure in the azimuthal direction through four slow-state variables, which details the amplitude, nature, and phase of the propagating acoustic pressure, simplifying the modal behavior dynamics. In this framework, the quaternion projection is utilized to depict the variations in acoustic pressure associated with azimuthal modes, as described by the following equation:

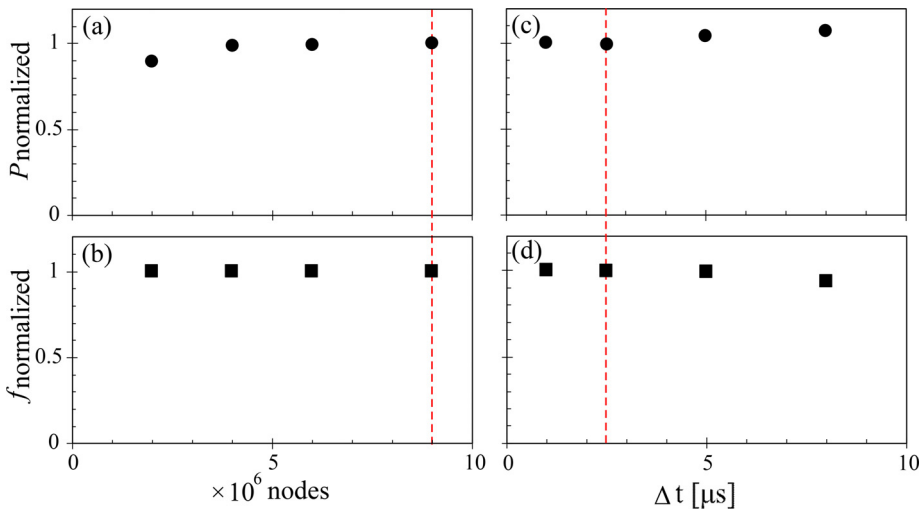


FIG. 4. Effect of (a) and (b) the number of grid nodes and (c) and (d) the time step size on the acoustic pressure amplitude and acoustic mode frequency in a square cavity at a flow velocity of 50 m/s. The dashed lines represent the conditions selected for this study.

26 July 2024 14:04:15

Published under an exclusive license by AIP Publishing

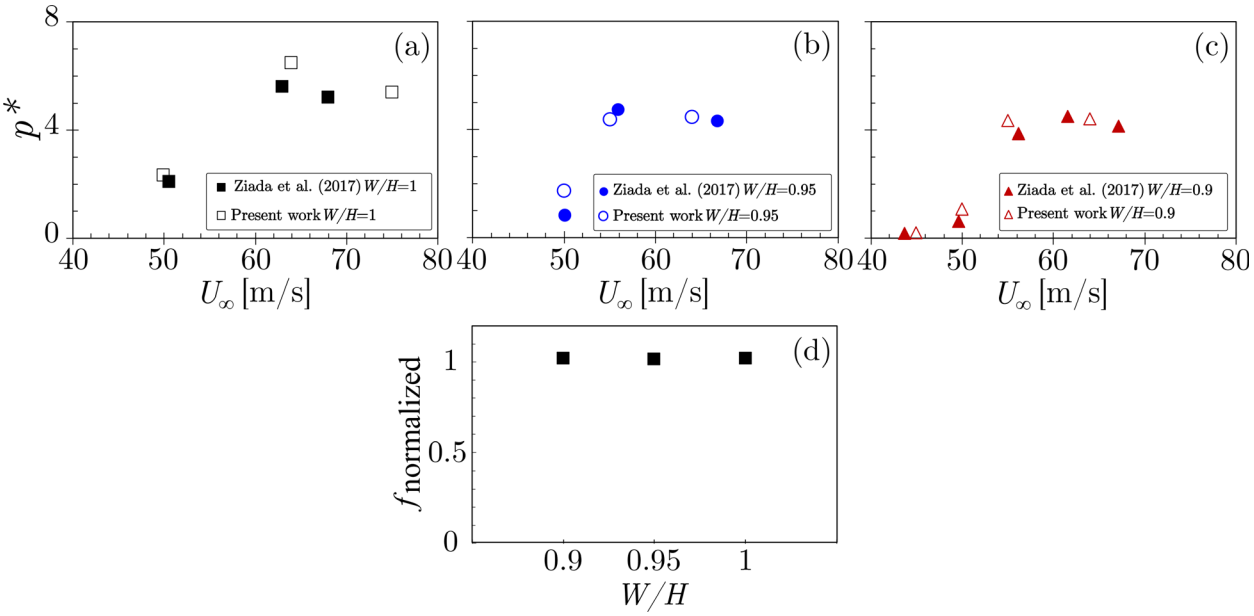


FIG. 5. Comparison of the model predictions for normalized acoustic pressure with the experimental results of Ziada *et al.*:[27] (a) $W/H = 1.0$, (b) $W/H = 0.95$, and (c) $W/H = 0.90$, and (d) the acoustic mode frequency for the three aspect ratios.

$$p(\theta,t) = A\cos(\Theta-\theta)\cos(\chi)\cos(\omega t+\phi) + A\sin(\Theta-\theta)\sin(\chi)\sin(\omega t+\phi). \quad (5)$$

Equation (5) defines the instantaneous state of the mode of frequency ω around azimuthal coordinate Θ through four slow variables A, χ, θ, and ϕ. Each variable captures specific characteristics of the acoustic mode, facilitating a comprehensive analysis of its properties and behavior. The scalar quaternion magnitude (A) is linked to the instantaneous amplitude of the acoustic pressure. Higher values of A indicate a stronger wave at that particular instant in time with a peak location dependent on the other quaternion parameters. The angle, χ, defines the nature of the acoustic mode, essentially distinguishing between standing and spinning modes. This provides insight into the propagation characteristics. It can also be regarded as an indication of the angular velocity by which an acoustic mode spins. In the case that $\chi = 0$, the mode is purely standing, indicating that the wave does not spin around the cavity center but rather oscillates in place. An azimuthal spinning in the clockwise direction has $\chi = \pi/4$, while $\chi = -\pi/4$ indicates counterclockwise spinning. Positive values of $\chi < \pi/4$ indicate mixed modes that can be decomposed into a stationary mode and one that is spinning in a clockwise direction, while negative values of χ signify counterclockwise spinning superimposed with a stationary mode. The angle, θ, is the orientation angle that indicates the direction of maximal acoustic pressure amplitude within the cavity. For stationary modes, θ points to the antinodal direction, where the wave amplitude reaches its peak. In the context of spinning or mixed modes, θ provides information about the orientation of these modes, revealing how the directional characteristics of the wave's propagation or standing patterns influence the acoustic pressure distribution. Finally, ϕ is the temporal phase that relates to the timing of the wave's oscillations. It indicates the phase shift of the acoustic wave at a given instant, offering insight into the wave's oscillatory behavior over time.

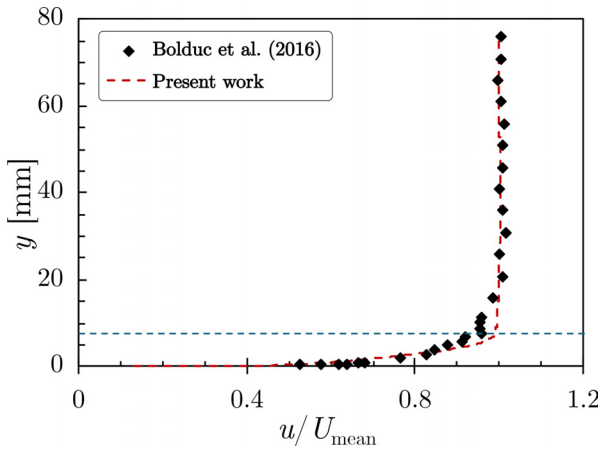


FIG. 6. Velocity profile at the upstream edge of the square cavity predicted by the LES in comparison with experimental measurements by Bolduc *et al.*[36] for the same cavity geometry.

III. SPINNING BEHAVIOR OF THE ACOUSTIC MODES

To identify the effect of small variations in the cavity aspect ratio on the excited acoustic resonance characteristics, the acoustic pressure is tracked on the cavity walls at different azimuthal angles. In each case, the simulation was given sufficient time to stabilize into a statistically steady state representing sustained acoustic resonance. Figure 7 provides samples of the acoustic pressure at the four corners of the cavity midspan where the peak acoustic pressure is observed for different W/H. The acoustic pressure time signal has a steady amplitude for

26 July 2024 14:04:15

Published under an exclusive license by AIP Publishing

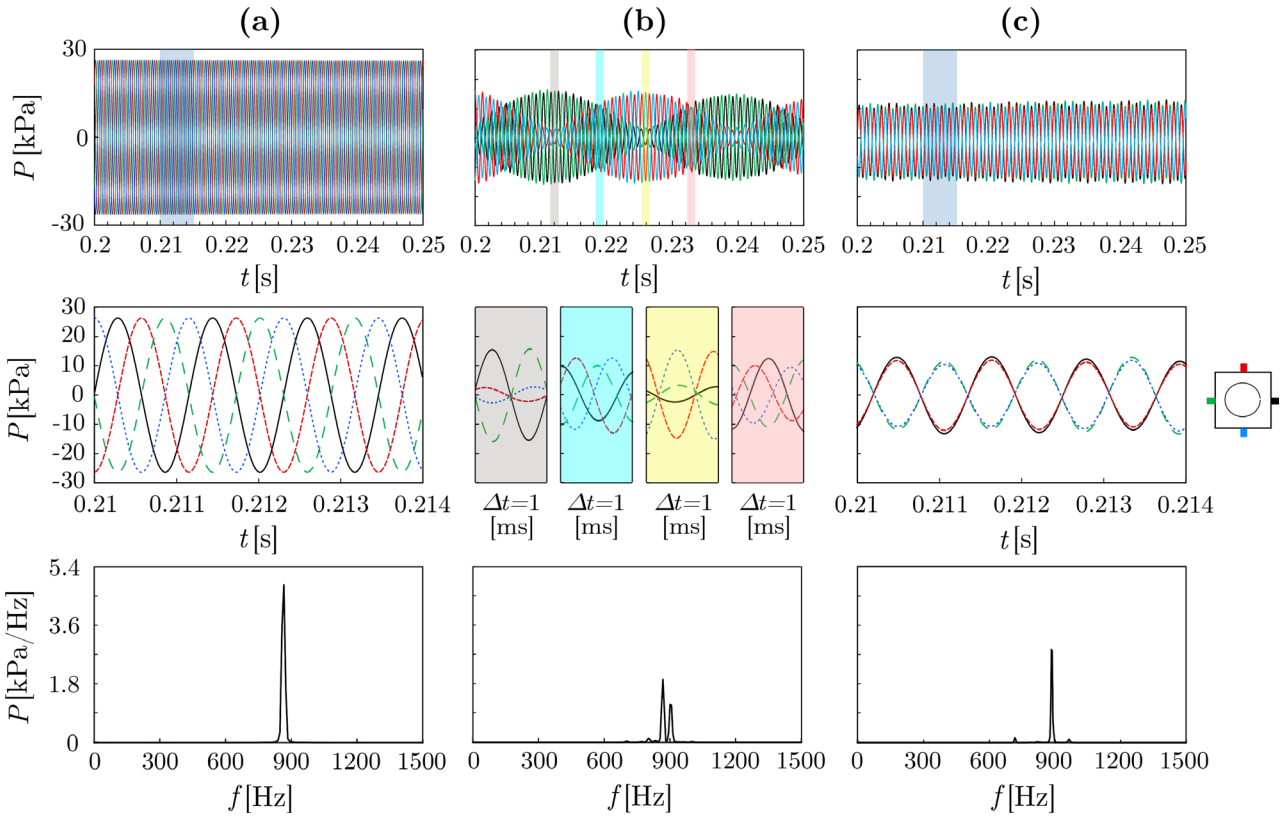


FIG. 7. Acoustic pressure signal at the corners of the cavity midspan, locations "—" P_1, "- -" P_3, "– –" P_5, and "...." P_7 in Fig. 2, for various cavity aspect ratios: (a) $W/H = 1.0$, (b) $W/H = 0.95$, and (c) $W/H = 0.90$, at a flow velocity of $U_\infty = 50$ m/s. Top row: time signal for a period of 0.05 s. Middle row: detailed time signal at segments highlighted earlier. Bottom row: The signal Amplitude Spectral Density (ASD).

both the square cavity ($W/H = 1$) and that with $W/H = 0.90$, while the case with $W/H = 0.95$ shows a beating frequency of about 40 Hz, much lower than the main acoustic frequency of about 900 Hz. Moreover, the amplitude at the corners of the cavity is much higher for the square case than the two other cases. This agrees with the experimental findings that a small deviation of W/H from unity can result in significant changes in the acoustic pressure amplitude. The detailed segments of the acoustic pressure signal shown in the middle row of Fig. 7 reveal a significant difference in the phase characteristics for the three cases. The square cavity ($W/H = 1$) excited a spinning azimuthal mode where the pressure at the four corners oscillates with the same frequency and amplitude with a phase shift of $\pi/2$ between each two successive corners. The acoustic mode for the cavity with $W/H = 0.90$ has two out-of-phase signal pairs with a time varying amplitude. For the aspect ratio $W/H = 0.95$, the beating acoustic pressure leads to an alternating pattern that involves both phase and amplitude, such that an increase in the acoustic pressure amplitude at certain corners is associated with a decrease in others. In addition, the phase between the pressure probes does not fully adhere to one of the two patterns described earlier, but rather, it alternates between them. In some sense, this case seems to behave with a blend of the characteristics of the two other cases, leading to the acoustic pressure beating. The dominant frequencies in the signals are indicated by the amplitude spectral density (ASD) shown at the bottom of Fig. 7. The aspect ratio change from 1.0 to 0.90 is not associated with any significant change in the frequency, but the median aspect ratio of 0.95 has two proximate frequencies, which is consequence of the beating behavior.

The spatial variation of the acoustic pressure phase is a major parameter in the energy exchange mechanism from the flow field to the excited acoustic mode. Figure 8 shows the phase relationship at points on the cavity circumference. The phase is shown for eight points located at equal azimuth angles, including the four corners and the four points on the middle of the sides. The phase of the acoustic pressure on the walls of the square cavity has equal phase differences of 45°, indicating an azimuthal mode that spins at a fixed rotational speed similar to that observed in the case of a circular axisymmetric cavity. This is an indication that the square cavity, while not radially symmetric, is able to sustain an azimuthal spinning mode. In contrast, the acoustic pressure in the case with the aspect ratio $W/H = 0.90$ occurs in two phase levels that are exactly out-of-phase with each other. Each of the two phase levels occurs over four adjacent points covering half of the cavity circumference. Such pattern is typical of a stationary acoustic mode that does not spin. Interestingly, the phase pattern for the median aspect ratio $W/H = 0.95$ changes over time, with a cycle. At the start of its cycle, the acoustic pressure phase continuously decreases as the azimuth angle increases. The phase pattern drifts such that, after a quarter of the beating cycle, a pattern pertaining to a stationary acoustic mode is observed. Analysis of pressure

26 July 2024 14:04:15

Published under an exclusive license by AIP Publishing

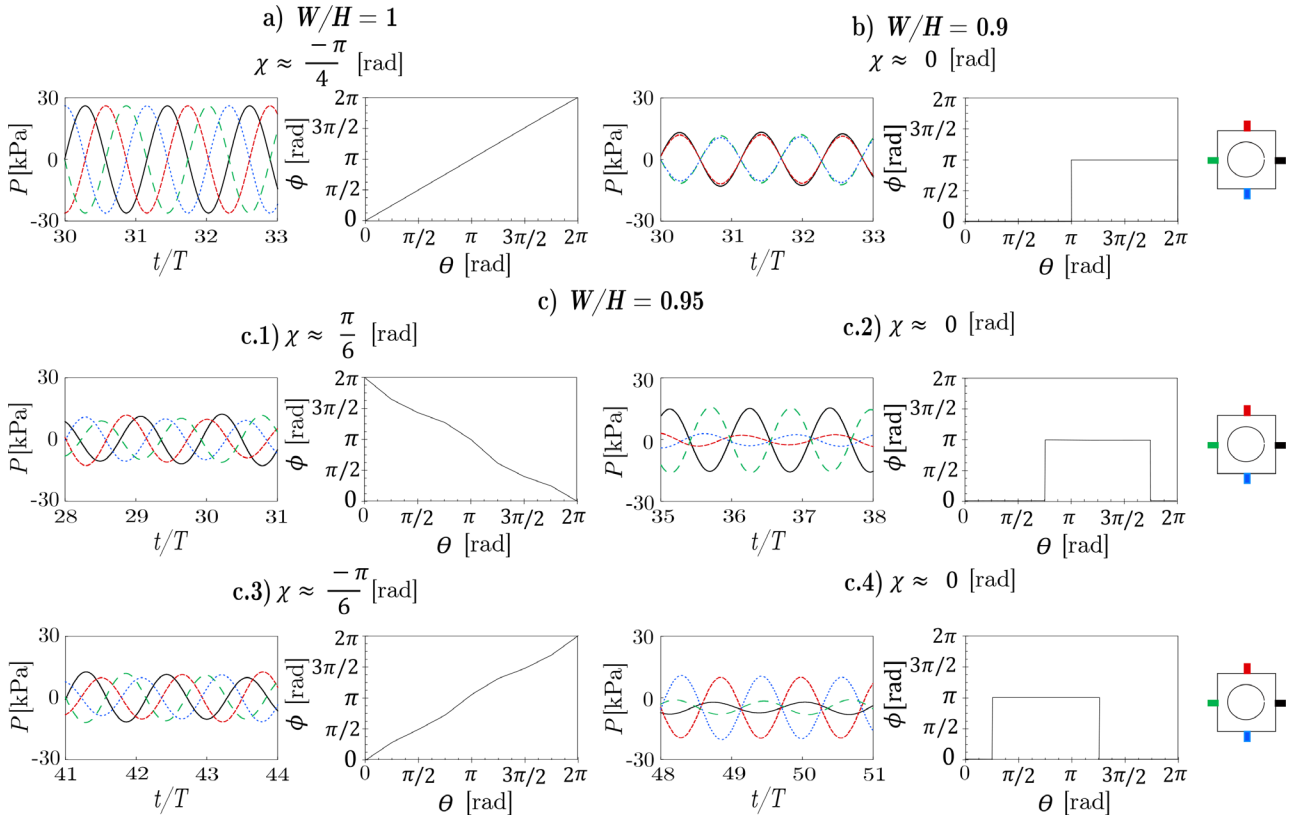


FIG. 8. Phase characteristics of the acoustic signal ("–"P_1, "- -"P_3, "– –"P_5, and "…."P_7 as depicted in Fig. 2) around the cavity circumference at midspan for (a) $W/H = 1.0$, (b) $W/H = 0.95$ at four different time instants, and (c) $W/H = 0.90$. T represents the period of the acoustic mode.

contours through simulation in the subsequent discussion provides compelling evidence supporting the presence of this phenomenon. In the next stage, the phase pattern reverses toward an increasing phase with an increasing azimuth angle, which indicates that the spinning direction has reversed. After another quarter beating cycle, the spinning stops again, and the phase shows the same stationary mode pattern.

Figure 9 shows the slow-state variables for the three cases at the same flow velocity. Figure 9(a) presents the raw static pressure signals from sensors P_2 and P_3 located at the upper right corner and the middle of the top wall of the cavity, respectively. Figure 9(b) shows that the amplitude, A, is much higher for the case of $W/H = 1.0$ than the other two cases and fluctuates slightly. The fluctuation of the amplitude is likely related to the square shape of the cavity because the amplitude is different when the peak is located at the corner or the side of the cavity section. The nature angle, χ, shown in Fig. 9(c) provides a quantitative indication of the spinning pace. For $W/H = 1.0$, the azimuthal mode is purely spinning in a counterclockwise direction. For the aspect ratio of $W/H = 0.95$, the value of the nature angle, χ, fluctuates between $\pi/4$ and $-\pi/4$, indicating that the spinning direction and pace changeover time. Conversely, the acoustic mode for the case with $W/H = 0.90$ is fixed close to its original reference. The spinning pace is indicated by a value of χ close to 0, indicating that the mode is stationary.

The orientation of the acoustic mode with respect to the reference location is reflected through the angle, θ, in Fig. 9(d). For $W/H = 1.0$, the continuous, perfectly linear increase in θ, spanning full rotations from $-\pi$ to π with time, highlights the steady spinning of the acoustic mode. For $W/H = 0.95$, θ changes in a cycle that oscillates between $-\pi$ and π in a periodic pattern, indicating that the orientation of the mode changes in cycles and reverses direction. Interestingly, the azimuthal mode periodically transitions from spinning to a halt, then spins in the opposite direction, then becomes stationary, and repeats this cycle. This periodic pattern does not appear to be purely sinusoidal but rather follows a pattern that points to an unstable or periodic flow behavior typical of turbulent bifurcation, mode switching, or wake oscillations, thus may depend on abrupt changes in the separating shear layer at the cavity mouth. For $W/H = 0.90$, the orientation angle, θ, is stable at its original value, indicating no spinning.

In Fig. 10, the state variables for different cavity W/H over time are represented on the Poincaré sphere. Each state is represented by a point such that the distance from the center is the amplitude, A, while two radial angles are represented by 2χ and 2θ. This representation provides information about the dynamic behavior of the mode in time when the state progression through time is used. States located near the poles denote spinning behavior, and circles around the equator are representative of pure standing waves, while other states can be decomposed into a superposition of both. In Fig. 10, the equator

26 July 2024 14:04:15

Published under an exclusive license by AIP Publishing

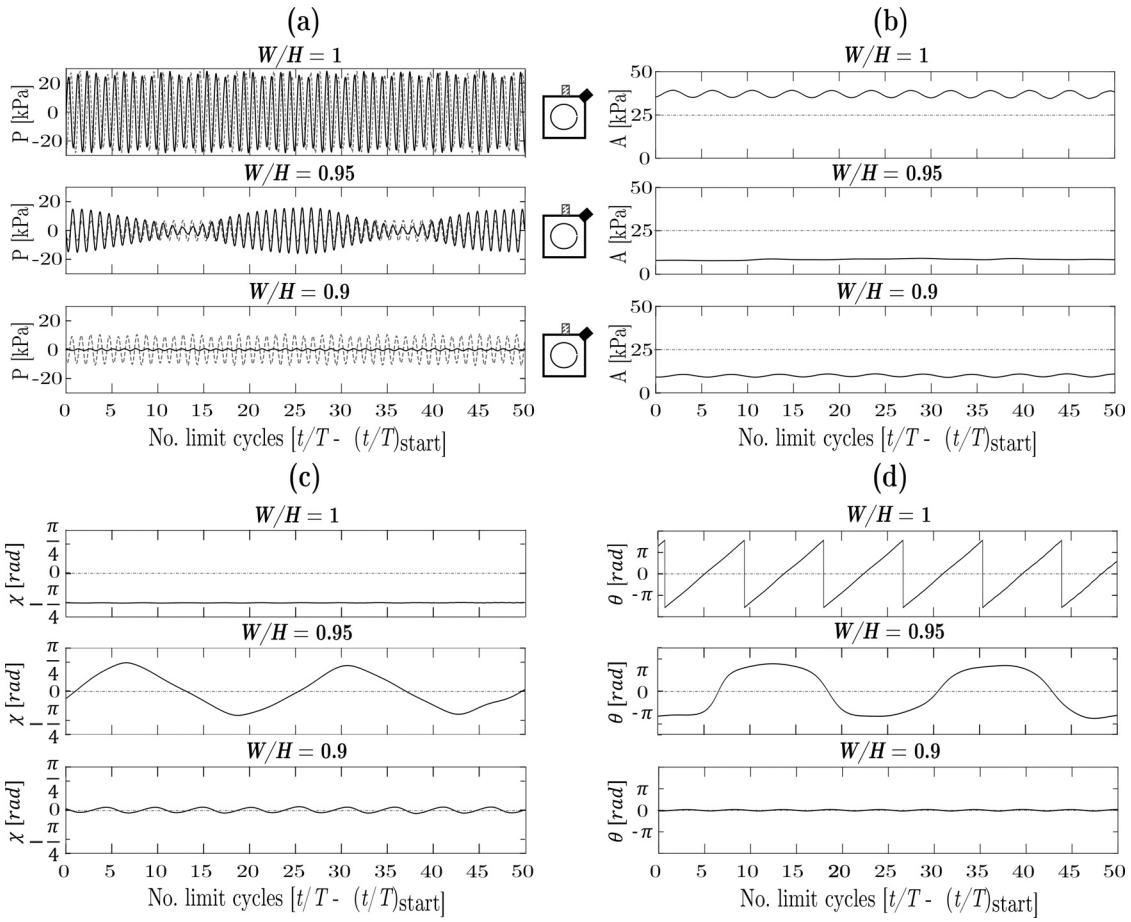


FIG. 9. (a) Pressure signals, and development of the slow-state variables (b) A, (c) χ, and (d) θ from two orthogonal pressure signal "—"P_2 and "- -"P_3 as illustrated in Fig. 2 for different cavity aspect ratios at the same upstream flow velocity of 50 m/s. T represents the period of the acoustic mode.

denotes purely standing waves, while positions at the north and south poles at the S_3 axis indicate waves rotating in the clockwise and counterclockwise directions, respectively. For the square cavity, the dynamic state is essentially stable near the pole at which $2\chi = \pi/2$, indicating a stable spinning mode. The acoustic resonance excited in the cavity with $W/H = 0.90$ has a pure stationary mode as indicated by the periodic state rotation with a fixed χ value of zero. The cavity with $W/H = 0.95$ has a state that alternates in both directions, toward the poles and also sideways such that both a stationary and spinning behavior characteristics are observed.

Instantaneous snapshots of the acoustic pressure field predicted by the LES model are shown in Fig. 11 over a cycle for different cavity configurations. For $W/H = 1.0$, the acoustic pressure at each corner of the cavity is periodic and has a fairly constant amplitude. Over a complete cycle, the acoustic pressure field exhibits a clear spinning behavior, where the peak of the acoustic pressure rotates around the cavity, and a pressure node is located at the center of the cavity. Due to the square shape of the cavity cross section, the amplitude tends to be higher when the peak is closer to the corners of the cavity, explaining the fluctuations in amplitude, A, in Fig. 9. For the case with $W/H = 0.95$, the acoustic mode pattern undergoes a periodic change, which occurs with a rate much slower than that of the main cycle, such that the acoustic pressure is at a different amplitude and frequency over time. Four distinctive patterns are shown in Fig. 11. At instant 1, the acoustic cycle is at its highest amplitude and frequency. The associated pressure field is nearly stationary and oscillates, such that the acoustic pressure antinodes occur at two opposite corners, and two nodes occur at the other pair of corners. At instant 2, where $\chi > 0$, the amplitude is lower than the stationary mode. The pressure field shows that the acoustic pressure of the mode is mostly spinning clockwise, albeit with a visible reduction in amplitude as the cycle progresses and the positive peak is located near the right corners. As the slow transition results in χ close to zero, the observed oscillating field is evidently stationary, but the peaks are located at the corners of the cavity, unlike the cavity with the lowest aspect ratio (i.e., $W/H = 0.90$) for which the peak acoustic pressure occurred on the short sides. After a few cycles, the value of χ becomes negative, and the spinning reverses to a counterclockwise direction. The cycle is complete when the value of χ reaches zero again, and the mode becomes stationary with the two other corners as the antinodes. Notably, the shape of the circular upstream and downstream cavity edges is visible in the acoustic pressure pattern for all configurations, which points to

26 July 2024 14:04:15

Published under an exclusive license by AIP Publishing

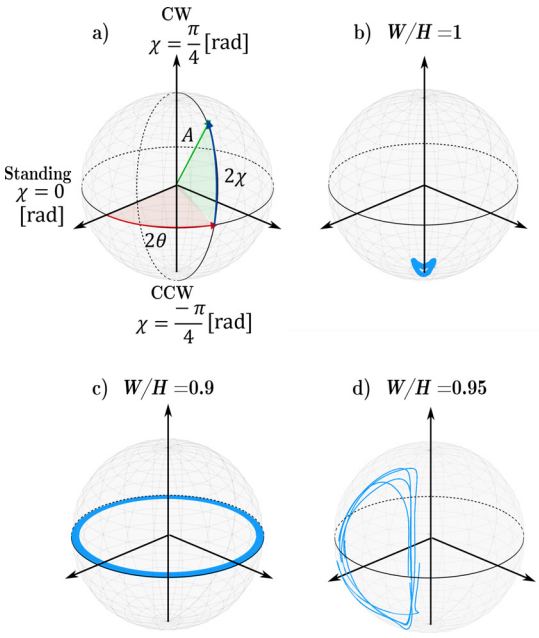


FIG. 10. (a) Variable specification, and Poincaré representation of the dynamic pressure oscillations across the circumference of the cavity midspan for (b) $W/H = 1.0$, (c) $W/H = 0.90$, and (d) $W/H = 0.95$.

their role in the interaction between the shear layer and the acoustic modes trapped within the cavity. Finally, at an aspect ratio $W/H = 0.90$, the cavity has a stationary mode with two opposite sides as the antinodal planes.

This behavior can be explained by analytically investigating the dynamic behavior of the two degenerate modes that constitute the fundamental rectangular cavity modes. For a rectangular cavity of dimensions L_x, L_y, and L_z with rigid walls, the acoustic pressure inside the cavity takes the modal form

$$p_{lmn} = A\cos\left(\frac{l\pi x}{L_x}\right)\cos\left(\frac{m\pi y}{L_y}\right)\cos\left(\frac{n\pi z}{L_z}\right)e^{j\omega_{lmn}t}, \tag{6}$$

where l, m, and n are the integer mode numbers in the x, y, and z coordinates, respectively. The natural angular frequency of the mode lmn is given by

$$\omega_{lmn} = c\left[\left(\frac{l\pi}{L_x}\right)^2 + \left(\frac{m\pi}{L_y}\right)^2 + \left(\frac{n\pi}{L_z}\right)^2\right]^{\frac{1}{2}}. \tag{7}$$

The spinning mode of the lowest frequency forms inside the cavity when the two modes $(l = 0, m = 1, n = 0)$ and $(l = 0, m = 0, n = 1)$ are superimposed with a phase shift of $\pi/2$. It follows that the ratio of the two degenerate mode frequencies is equal to the ratio W/H. For a cavity with an aspect ratio $W/H = 1.0$, those two degenerate modes are equal in frequency while for a cavity with $W/H = 0.95$, the two modes are asynchronous. In Fig. 12, the two-dimensional acoustic pressure field calculated from Eq. (6) with a phase shift of $\pi/2$ results in a clear spinning behavior. Modes A and B are equal in frequency, and the resulting mode spins in a counterclockwise direction. The direction of spinning in this case depends entirely on the prescribed phase shift. In this case of complete frequency match, the phase shift is related to the behavior of the flow field at the separation edge and may be sensitive to small acoustic perturbations or effects of turbulence.

In contrast, Eq. (6) predicts an acoustic field with rich dynamics when the two superimposed modes $(l = 0, m = 1, n = 0)$ and $(l = 0, m = 0, n = 1)$ are mismatched in frequency. The upper side of Fig. 13 shows the values of the amplitudes at the cavity corner, indicating a beating dynamic identical to that observed in Fig. 9. The details of the degenerate fields and their superposition are shown at four instants. In instant 1, the acoustic pressure of the two modes is in phase at the right upper corner, and the result is a stationary behavior, with the peak at that corner. At instant 2, the phases are shifted with about $\pi/2$ at the upper right corner, and the superposition is spinning clockwise. At instant 3, the pressure at the right upper corner is out of phase, and the superposition is a stationary mode with a pressure peak at the two other opposite corners. At instant 4, the spinning direction is reversed to become counterclockwise, as the phase difference is negative its value of instant 2. This analysis shows that the spinning direction and reversal behavior are a feature of the acoustic field alone, as it results from a transient change in the superimposed mode phase, which is a feature of the geometry and not the flow field. It is important to note that Eq. (6) predicts the same reversal of direction if the deviation of frequency grows wider to a ratio of 0.9, despite the model prediction that the behavior of the cavity acoustic mode did not follow a spinning pattern. This can be explained when the interaction of the flow field and the acoustic field is considered. To excite two degenerate modes simultaneously, the shear layer separation and impingement process must be able to lock-in to the two modes. While the acoustic modes may be able to force a lock-in on the shear layer and cause it to shift its phase and frequency, this capability has limits, and the lock-in breaks down when the frequency of the shear layer is sufficiently different from that of the acoustic mode. Thus, a limit exists, observed here to be between 5% and 10% of the shear layer oscillation frequency, beyond which only one of the two degenerate modes will get excited and the other will not, resulting in a stationary mode. A consequence of this behavior is that for the case with $W/H = 0.9$, the antinode of acoustic pressure occurs parallel to the short side, as it represents the antinode for the excited mode. In contrast, the stationary instant at the spinning reversal case $W/H = 0.95$ has the antinode passing between two corners, as the two degenerate modes are equal in strength at that instant. The interaction between the shear layer and the acoustic mode will be discussed in detail in Sec. IV.

IV. SHEAR LAYER DYNAMICS

As the energy source is closely linked to the fluctuations of pressure resulting from shear layer impingement, the shear layer dynamics over the mouth of the rectangular cavity cross section plays an important role that enables the excitation of the acoustic modes observed. Due to the variety of features noted for the acoustic mode, it is interesting to inspect how responsive the shear layer is to changes in amplitude and spinning direction of the acoustic mode to maintain an effective coupling that generates net acoustic energy over the cycle. In Figs. 14–17, multiple aspects of the shear flow are demonstrated for the three cavity configurations under consideration. Figure 14 demonstrates the vortex separation dynamics for the cavity with a square cross section $W/H = 1.0$. The shear layer is present in the form of a

26 July 2024 14:04:15

Published under an exclusive license by AIP Publishing

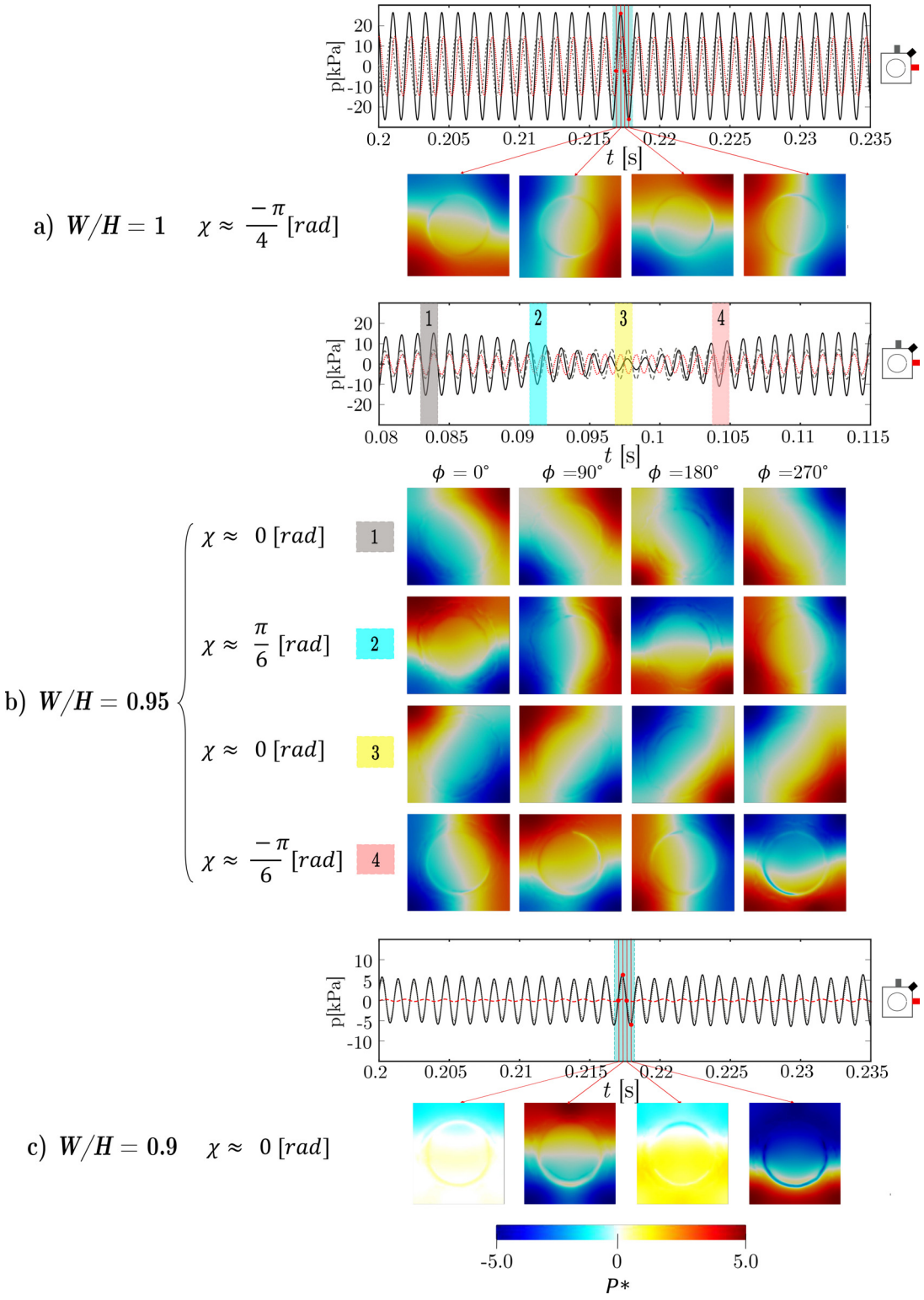


FIG. 11. Instantaneous normalized acoustic pressure signals p^* and the associated pressure fields predicted by Large Eddy Simulation at four equidistant instants during the acoustic cycle at the same upstream velocity $U = 50$ m/s for (a) $W/H = 1.0$, (b) $W/H = 0.95$, and (c) $W/H = 0.90$.

26 July 2024 14:04:15

Published under an exclusive license by AIP Publishing

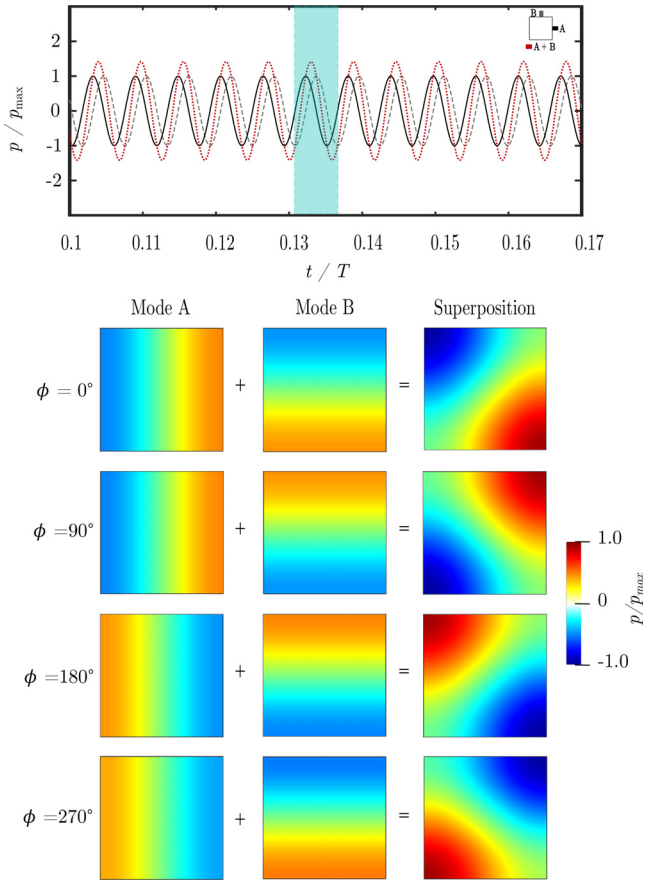


FIG. 12. The two degenerate acoustic modes and their superposition at different cycle instants for the case of $W/H = 1.0$ as predicted by Eq. (6). Top: pressure signal at two adjacent sides. Bottom: pressure field at different phases.

helix that extends across the cavity as a single loop, such that the separation and impingement points occur at the same $x - y$ streamwise plane. Upon impingement, the vortex deforms and breaks down into irregular vortices that get conveyed downstream. The vorticity fields at the four corner planes show that, at the same time instant within the cycle, a single vortex core is at different locations between the leading and trailing edges. Moreover, the synchronous timing of impingement at the same plane with the separation of the next vortex core is typical for the first shear layer mode over the cavity edge. The right side of Fig. 14 shows the superposition of the acoustic pressure field with the helical vortex core over an acoustic cycle. A major aspect is that the separation and impingement occur at an orientation angle θ that corresponds to the same value of acoustic pressure at all phases. This creates a persistent phase difference between the acoustic field and flow fluctuations necessary for energy transfer, which signifies the relationship of impingement to the generation of the acoustic energy. During lock-in, acoustic oscillations are synchronized with the fluctuations induced by impingement, therefore sustaining the spinning mode. Over the cycle, spinning continuously rotates the orientation of this process, facilitated by the axisymmetric shape of the leading and separation edges. Due to spinning, the impingement of the shear layer occurs at orientations with a varying peak level of acoustic pressure, explaining the fluctuating amplitude.

While evidently different, the shear layer dynamics during the excitation of a stationary azimuthal mode for the rectangular case of $W/H = 0.9$ share important features with the spinning case. In Fig. 15, the vortex core takes the form of two subsequent and opposite crescents, split at the orientation angle $\theta = 0$. The two crescents are aligned with the two antinodal sides of the acoustic pressure field. This allows only a single vortex to separate and impinge on the edges over the area where significant acoustic oscillations are observed. Similar to the spinning case, separation and impingement is synchronized such that the lock-in mechanism stays in effect, sustaining resonance. The difference is that, rather than a rotating point, synchronization occurs over a semicircle. Thus, the two opposite crescent vortices impinge with a phase delay of π, the same phase delay between the two acoustic pressure antinodes. The acoustic pressure superposition with the vortex core offers an insight on the potential cause of amplitude reduction. The acoustic pressure peak occurs at the corners, while the shear layer crescent is most organized away from its edges, middle of the edge side. This may have reduced the potential of energy transfer during lock-in between the maximum fluctuations induced by the vortex impingement and the peak acoustic pressure.

Aspects of the shear layer dynamics for the case $W/H = 0.95$ in the instant where the acoustic mode becomes momentarily stationary are illustrated in Fig. 16. While this occurs in two extreme points in the cycle, the two are mirrors of one another that show the same behavior, just with an opposite phase and orientation. As the stationary acoustic mode is excited with its antinodal planes passing by the corners, the separating vortex takes the form of two crescents that are split by the cavity diagonal plane. Most features that are present in the stationary case of $W/H = 0.90$ are still observed. First, the crescents are oriented such as impingement of their middle point occurs at the orientation of the peak acoustic amplitude, at two opposite corners. As the vortices at the peak acoustic pressure corners $\theta = 3\pi/4$ and $\theta = 7\pi/4$ are strong and well organized, while the vortices at the pressure node diagonal plane are much weaker, the impingement orientation optimizes the generation of acoustic oscillations. Second, the separation and impingement are spaced by a phase delay of 2π such that exactly a single vortex core is observed over the cavity mouth. Moreover, vortices in the two diagonal sides of the cavity are separated by half the cavity streamwise length, representing a phase shift of π for the first shear layer mode.

As the acoustic mode spins, the shear layer dynamics for the same case $W/H = 0.95$ transition to resemble the spinning dynamics observed for the square cavity case $W/H = 1.0$ shown in Fig. 14. Figure 17 illustrates the dynamic features of the shear layers for the two cases when the acoustic pressure is rotating counterclockwise and clockwise. The figure shows a lot of similarity between the two cases. For both cases, the vortex core is a helix extending between the leading and trailing edges. Therefore, vortices at different orientations are located at different distances from the upstream and downstream edges. Shear layer separation and impingement are spaced by a complete acoustic cycle, indicating that lock-in is synchronizing the process. Evidently, separation and impingement points have the same orientation angle θ with the acoustic pressure mode as both spin in the azimuthal direction. The major difference is that, when looked upon from the upstream side, the helix appears to be rotating in two

26 July 2024 14:04:15

Published under an exclusive license by AIP Publishing

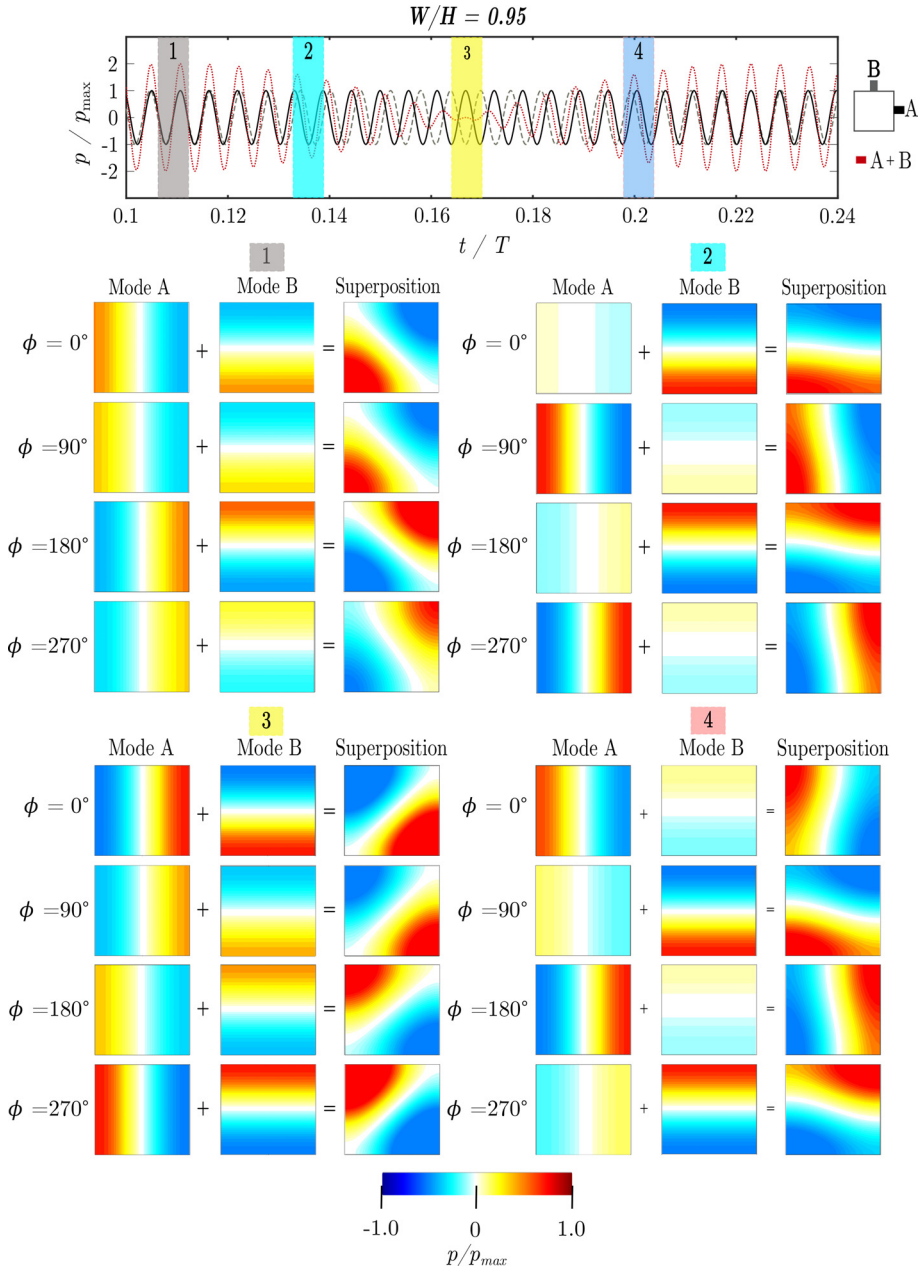


FIG. 13. The two degenerate acoustic modes and their superposition at different cycle instants for the case of $W/H = 0.95$ as predicted by Eq. (6). Top: pressure signal at two adjacent sides. Bottom: pressure field at different spinning behavior and acoustic cycle phases.

opposite directions in Figs. 17(a) and 17(b), corresponding to the opposite rotating directions of the acoustic pressure.

The transient behavior in the case of $W/H = 0.95$ is slow relative to the acoustic mode frequency such that the shear layer transitions from a helix shape to the form of two semi-circular cores and back in a cycle, exhibiting the behavior patterns in Figs. 16 and 17, and transitional patterns between them. As the orientation of the acoustic pressure is spinning clockwise, the vortex core separates in the form of a helix such that the separation point, the red point in Fig. 17(b), spins around the leading edge clockwise. As the frequency shift of the two degenerate modes result in an instant where the spinning of the acoustic mode stops momentarily, the vortex cores have deformed into two separate crescents, as seen in Fig. 16. Next, the reversal of spinning direction causes the shear layer separation to create a helical shape in which the separation point spins in the counterclockwise direction, as in Fig. 17(a). The cycle concludes when the spinning stops momentarily, coinciding with the separation of crescent vortex cores and their impingement on the cavity edges, which occurs at two corners different from those observed earlier. This peculiar feature of the shear layer spinning cannot be explained by an influence of the mean flow swirl,

26 July 2024 14:04:15

Published under an exclusive license by AIP Publishing

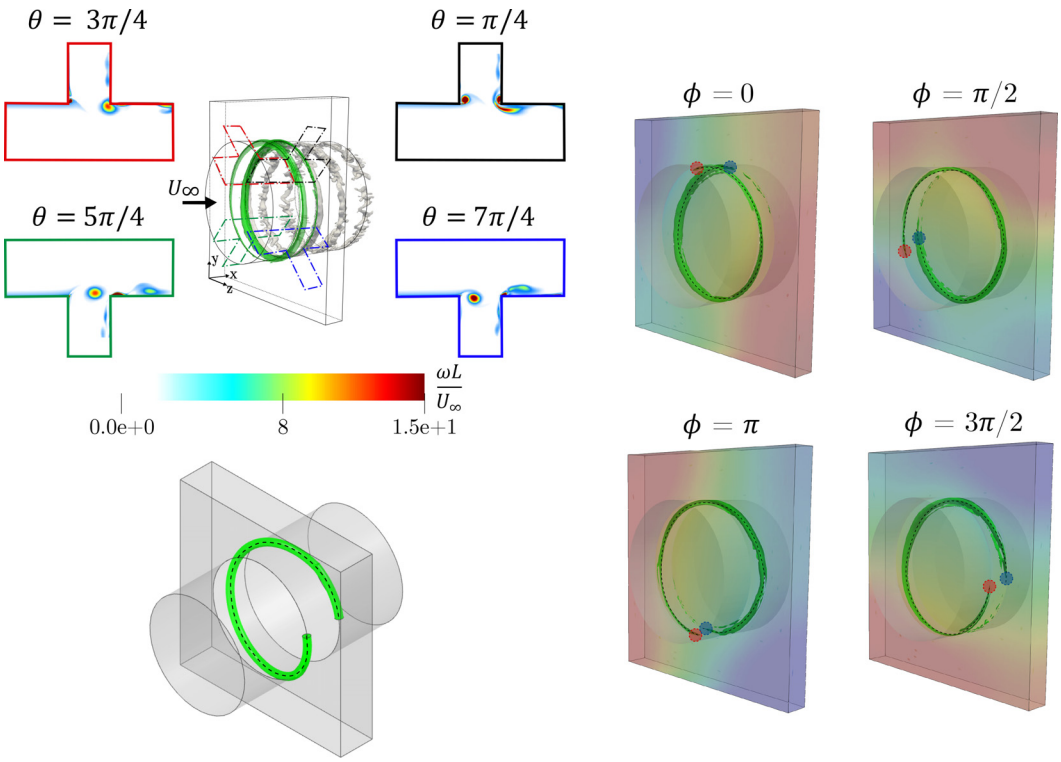


FIG. 14. The shear layer dynamics for the square cavity with $W/H = 1.0$. Top left: Q-criterion isosurface and vorticity snapshots at the four corner planes. Bottom left: A schematic representation of the vortex shape. Right: Separating vortex development over an acoustic cycle superimposed on the acoustic pressure. The red and blue points are separation and impingement locations, respectively. The flow velocity is left to right.

as the flow uniformly originates from the inlet, and, thus, any swirl is influenced and caused by the shear layer dynamics and not the other way around. Similarly, the asymmetry of the cavity is imposed by its rectangular shape and cannot explain a tendency of the shear layer to separate in a particular direction then its opposite. The transient behavior in the case of $W/H = 0.95$ is not abrupt or intermittent but rather continuous and persistent, eliminating turbulence as a determining factor. Therefore, it can be inferred that the acoustic mode tendency to periodically reverse its spin due to the superposition of two degenerate modes of slightly mismatched frequencies drives the feedback mechanism, imposes the necessary timing on the shear layer, and determines the separation and impingement dynamics. While it has been demonstrated before that disrupting the shear layer dynamics by flow obstructions may alter the coupling mechanism, the insight from the current configuration brings modifications targeted at the acoustic mode characteristics of the flow into focus. A small mismatch in frequencies due to small deviations in lengths may be responsible for slow transactional dynamics and can explain the observed reversal of the spinning direction. More importantly, a larger mismatch induced by tailoring the cavity dimensions can be effective in mitigating the spinning dynamics and lowering the amplitude of the resultant oscillations.

V. CONCLUSION

The shear layer separating at an axisymmetric leading edge of a shallow cavity may become unstable before it impinges on the opposite trailing edge, coupling with the cavity acoustic modes that coincide with its oscillation frequency. Under certain conditions, this flow-acoustic coupling may lead to the excitation of stationary or spinning azimuthal modes, resonating and generating high noise and vibration. In this study, the spinning behavior of self-excited azimuthal acoustic modes in a rectangular cavity with opposite axisymmetric upstream and downstream leading edges is numerically investigated. A rectangular cavity with opposite axisymmetric leading and trailing edges is modeled using compressible large eddy simulation (LES) with temporal and spatial resolutions sufficient to self-excite the fundamental acoustic modes of the cavity. Three aspect ratios were considered for the rectangular cavity to control the frequency mismatch of the two fundamental degenerate modes that add up to the spinning behavior. Results confirmed the significant role of the frequency mismatch in the spinning dynamics of the azimuthal acoustic mode, demonstrating the mechanism that explains the reversal of spinning direction. For the square cavity, the frequencies of the two degenerate modes are completely matched, allowing a spinning shear layer to excite them simultaneously, thereby exciting a continuously spinning azimuthal mode. A frequency mismatch of 5% (i.e., when the cavity aspect ratio is $W/H = 0.95$) enables the shear layer separating at the leading edge to excite the two degenerate modes simultaneously, resulting in a slow transition in the phase between them. This continuous phase change allows the spinning direction to change periodically, such that the separation point spins, slows down, and then comes to a stop manifesting

26 July 2024 14:04:15

Published under an exclusive license by AIP Publishing

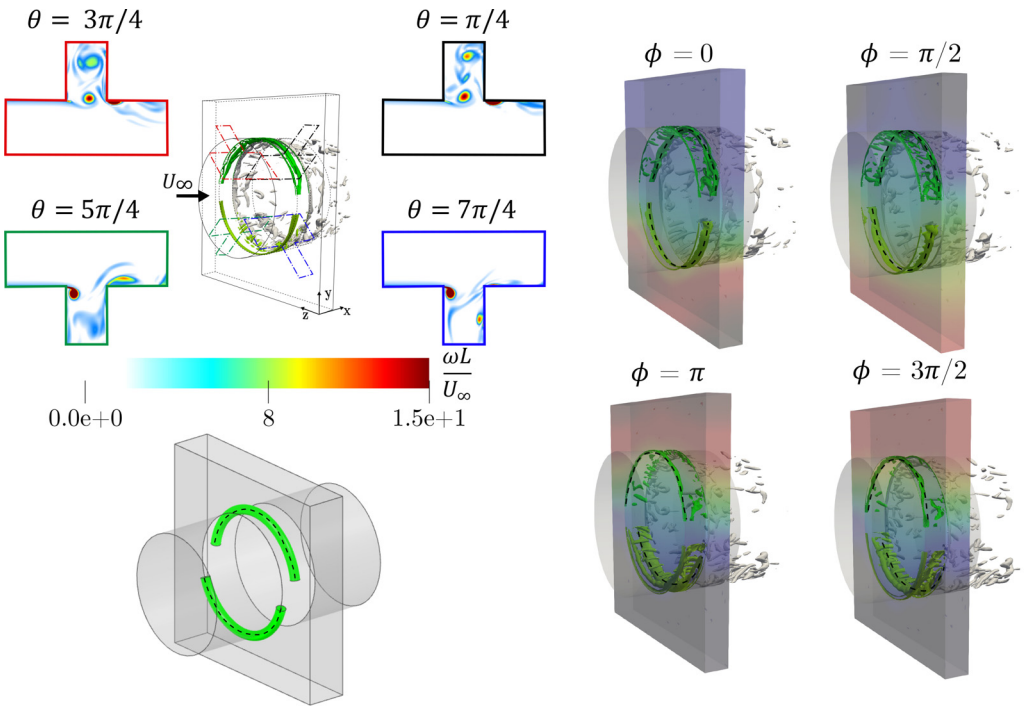


FIG. 15. The shear layer dynamics for the case $W/H = 0.90$.

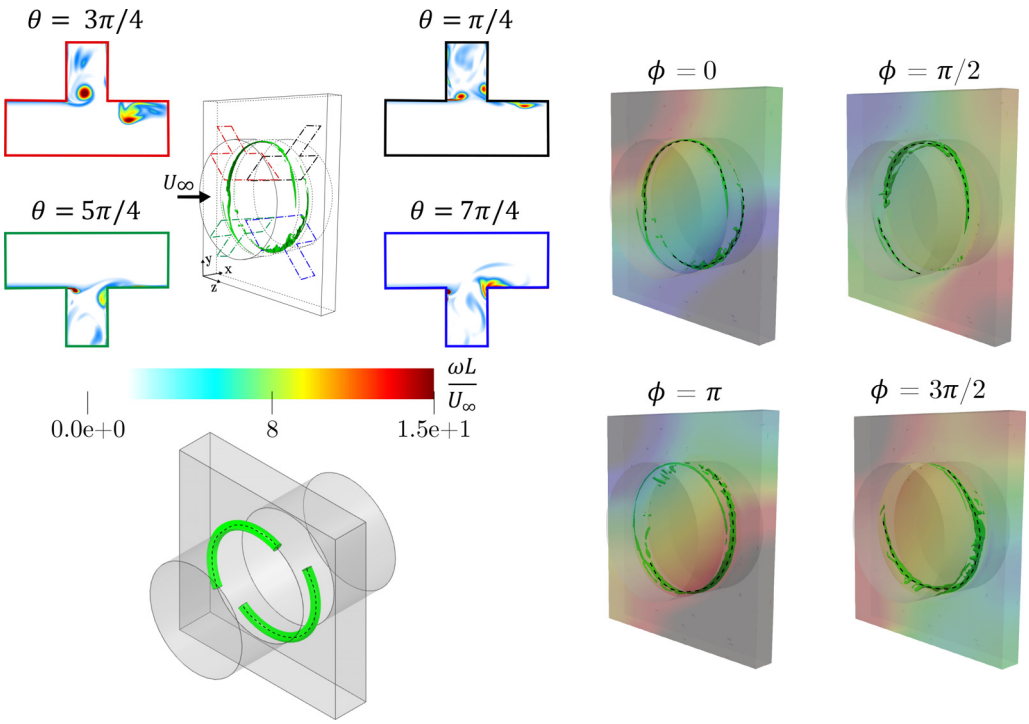


FIG. 16. The shear layer dynamics for the case $W/H = 0.95$ at $\chi = 0$.

26 July 2024 14:04:15

Published under an exclusive license by AIP Publishing

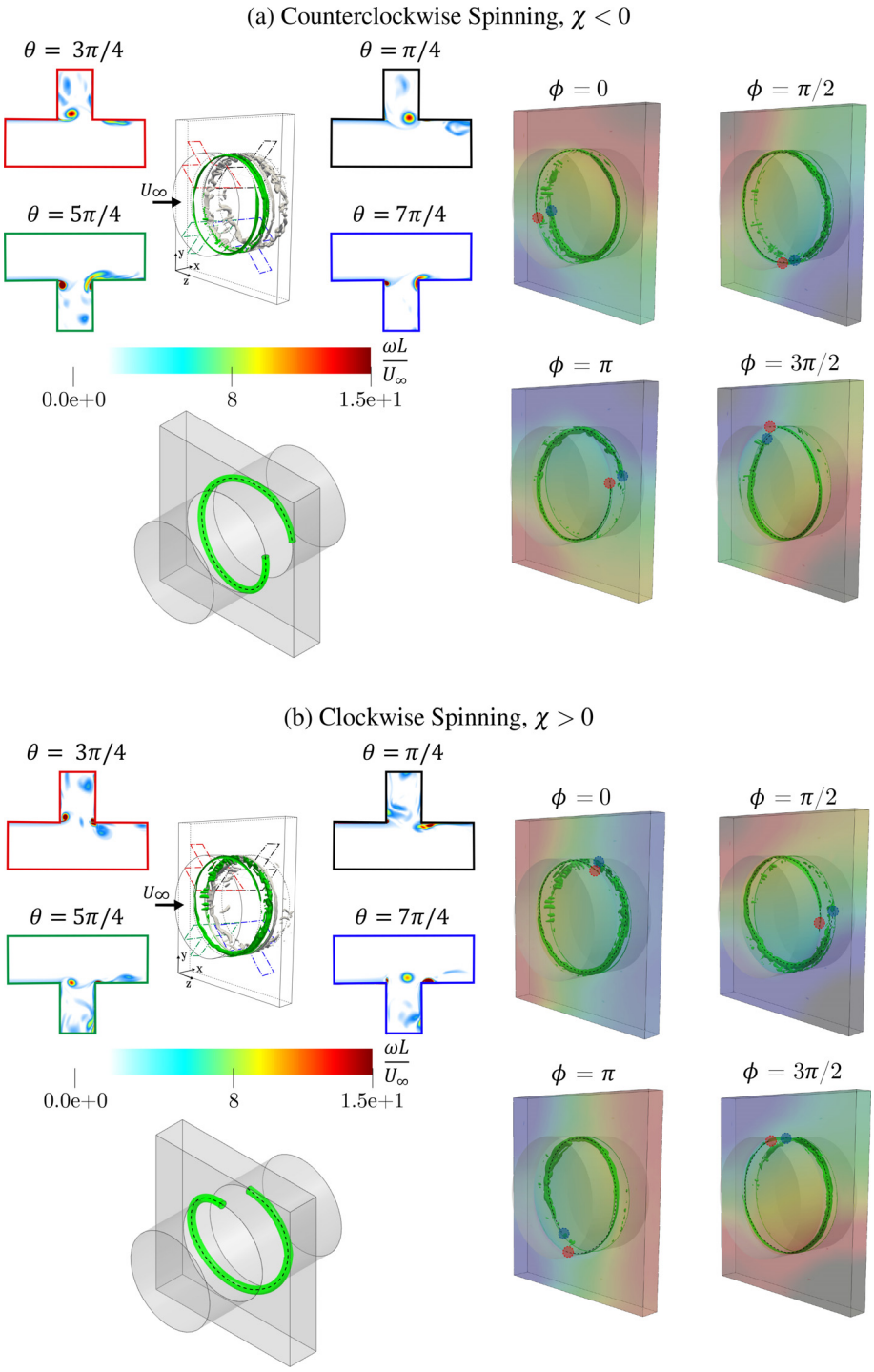


FIG. 17. The shear layer dynamics for the case $W/H = 0.95$ when the acoustic mode is (a) rotating counterclockwise, $\chi < 0$, and (b) rotating clockwise, $\chi > 0$.

itself as an instantaneously stationary mode. The spinning then reverses to the other direction, followed by another stop. This behavior is periodic and results in a beating amplitude of the acoustic pressure. If the aspect ratio of the cavity is higher such that the shear layer is not able to lock-in with the two modes simultaneously, only one of the two degenerate modes is excited, and a stationary acoustic mode is excited at a lower amplitude. The shear layer traveling across the cavity mouth follows the excited acoustic mode in each case. For the square cavity ($W/H = 1$), the separation and impingement points spin regularly creating a helical vortex. For the case with $W/H = 0.90$, where a

26 July 2024 14:04:15

Published under an exclusive license by AIP Publishing

stationary mode is excited, crescent vortices alternately separate and impinge over the edges. For the case with $W/H = 0.95$, the pace of rotation of the separation point across the leading edge changes over time. In this case, the shape of the vortex across the cavity continuously changes to follow the acoustic mode, indicating that a lock-in with this complex acoustic mode is still possible.

AUTHOR DECLARATIONS

Conflict of Interest

The authors have no conflicts to disclose.

Author Contributions

Mahmoud Shaaban: Conceptualization (equal); Data curation (equal); Formal analysis (equal); Investigation (equal); Methodology (equal); Visualization (equal); Writing – original draft (lead). **Rasha Noufal:** Conceptualization (equal); Data curation (equal); Formal analysis (equal); Methodology (equal); Software (lead); Validation (lead); Visualization (equal); Writing – original draft (equal). **Mohammed Alziadeh:** Data curation (equal); Investigation (equal); Methodology (equal); Writing – original draft (equal). **Atef Mohany:** Conceptualization (lead); Funding acquisition (lead); Investigation (equal); Methodology (lead); Project administration (lead); Supervision (lead); Visualization (equal); Writing – review & editing (lead).

DATA AVAILABILITY

The data that support the findings of this study are available from the corresponding author upon reasonable request.

REFERENCES

[1]H. Mohammed Al-Muslim, N. Ibrahim Al-Nasri, and M. Y. Al-Hashem, "The danger of piping failure due to acoustic-induced fatigue in infrequent operations: Two case studies," J. Pressure Vessel Technol. **135**, 064501 (2013).

[2]A. Omer, N. Arafa, A. Mohany, and M. Hassan, "The effect of upstream edge geometry on the acoustic resonance excitation in shallow rectangular cavities," Int. J. Aeroacoust. **15**, 253–275 (2016).

[3]P. Wang, Y. Deng, and Y. Liu, "Vortex dynamics during acoustic-mode transition in channel branches," Phys. Fluids **31**, 085109 (2019).

[4]M. Abdelmwgoud, M. Shaaban, and A. Mohany, "Flow dynamics and azimuthal behavior of the self-excited acoustic modes in axisymmetric shallow cavities," Phys. Fluids **32**, 115109 (2020).

[5]M. Abdelmwgoud, M. Shaaban, and A. Mohany, "Shear layer synchronization of aerodynamically isolated opposite cavities due to acoustic resonance excitation," Phys. Fluids **33**, 055112 (2021).

[6]M. Hanna and A. Mohany, "Aeroacoustics and shear layer characteristics of confined cavities subject to low Mach number flow," J. Fluids Struct. **121**, 103949 (2023).

[7]A. Oengoren and S. Ziada, "An in-depth study of vortex shedding, acoustic resonance and turbulent forces in normal triangle tube arrays," J. Fluids Struct. **12**, 717–758 (1998).

[8]J. R. Dawson and N. A. Worth, "Flame dynamics and unsteady heat release rate of self-excited azimuthal modes in an annular combustor," Combust. Flame **161**, 2565–2578 (2014).

[9]Y. Uchiyama and R. Morita, "Combined effects of steam wetness and pressure on characteristics of acoustic resonance amplitude in closed side branch," J. Pressure Vessel Technol. **143**, 011402 (2021).

[10]D. Rockwell and E. Naudascher, "Review—Self-sustaining oscillations of flow past cavities," J. Fluids Eng. **100**, 152–165 (1978).

[11]J. Keller and M. Escudier, "Flow-excited resonances in covered cavities," J. Sound Vib. **86**, 199–226 (1983).

[12]S. Ziada and P. Lafon, "Flow-excited acoustic resonance excitation mechanism, design guidelines, and counter measures," Appl. Mech. Rev. **66**, 010802 (2014).

[13]M. R. Islam, M. Shaaban, and A. Mohany, "Vortex dynamics and acoustic sources in the wake of finned cylinders during resonance excitation," Phys. Fluids **32**, 075117 (2020).

[14]K. Aly and S. Ziada, "Review of flow-excited resonance of acoustic trapped modes in ducted shallow cavities," J. Pressure Vessel Technol. **138**, 040803 (2016).

[15]J. Xu, J. Lei, J. Wu, and K. Zhang, "The three-dimensional characteristics of the unsteady wall-pressure in a low-Mach-number rectangular cavity flow with Rossiter model oscillation," Exp. Fluids **58**, 109 (2017).

[16]T. C. Lieuwen and V. Yang, *Combustion Instabilities in Gas Turbine Engines: Operational Experience, Fundamental Mechanisms, and Modeling* (American Institute of Aeronautics and Astronautics, 2006).

[17]A. Faure-Beaulieu, T. Indlekofer, J. R. Dawson, and N. Noiray, "Experiments and low-order modelling of intermittent transitions between clockwise and anticlockwise spinning thermoacoustic modes in annular combustors," Proc. Combust. Inst. **38**, 5943–5951 (2021).

[18]M. Bauerheim, P. Salas, F. Nicoud, and T. Poinsot, "Symmetry breaking of azimuthal thermo-acoustic modes in annular cavities: A theoretical study," J. Fluid Mech. **760**, 431–465 (2014).

[19]R. Parker, "Acoustic resonances and blade vibration in axial flow compressors," J. Sound Vib. **92**, 529–539 (1984).

[20]D. Evans, M. Levitin, and D. Vassiliev, "Existence theorems for trapped modes," J. Fluid Mech. **261**, 21–31 (1994).

[21]R. Parker, "Resonance effects in wake shedding from parallel plates: Calculation of resonant frequencies," J. Sound Vib. **5**, 330–343 (1967).

[22]R. Parker, "Resonance effects in wake shedding from parallel plates: Some experimental observations," J. Sound Vib. **4**, 62–72 (1966).

[23]K. Awny and S. Ziada, "Flow excitation of diametral acoustic modes of axisymmetric cavities," in *ASME Pressure Vessels and Piping Conference* (ASME, 2006), Vol. 47888, pp. 115–123.

[24]S. Hein, W. Koch, and L. Nannen, "Trapped modes and fano resonances in two-dimensional acoustical duct–cavity systems," J. Fluid Mech. **692**, 257–287 (2012).

[25]K. Aly and S. Ziada, "Azimuthal behaviour of flow-excited diametral modes of internal shallow cavities," J. Sound Vib. **330**, 3666–3683 (2011).

[26]K. Aly and S. Ziada, "Effect of mean flow on the trapped modes of internal cavities," J. Fluids Struct. **33**, 70–84 (2012).

[27]S. Ziada, M. Bolduc, and P. Lafon, "Flow-excited resonance of diametral acoustic modes in ducted rectangular cavities," AIAA J. **55**, 3817–3830 (2017).

[28]A. A. Shaaban and S. Ziada, "Effect of the separation distance on the aeroacoustic source of multiple shallow cavities," J. Fluids Eng. **141**, 011102 (2019).

[29]P. Wang and Y. Liu, "Influence of diametral acoustic mode on cavity flow dynamics: Zonal large eddy simulation and proper orthogonal decomposition," Phys. Fluids **32**, 075103 (2020).

[30]P. Wang and Y. Liu, "Spinning behavior of flow-acoustic resonant fields inside a cavity: Vortex-shedding modes and diametral acoustic modes," Phys. Fluids **32**, 085109 (2020).

[31]A. Faure-Beaulieu, Y. Xiong, T. Pedergnana, and N. Noiray, "Self-sustained azimuthal aeroacoustic modes. Part 1. Symmetry breaking of the mean flow by spinning waves," J. Fluid Mech. **971**, A21 (2023).

[32]A. Faure-Beaulieu, T. Pedergnana, and N. Noiray, "Self-sustained azimuthal aeroacoustic modes. Part 2. Effect of a swirling mean flow on the modal dynamics," J. Fluid Mech. **971**, A22 (2023).

[33]C. Y. Lee and S. Cant, "Assessment of LES subgrid-scale models and investigation of hydrodynamic behaviour for an axisymmetrical bluff body flow," Flow, Turbul. Combust. **98**, 155–176 (2017).

[34]A. K. Shukla and A. Dewan, "OpenFOAM based LES of slot jet impingement heat transfer at low nozzle to plate spacing using four SGS models," Heat Mass Transfer **55**, 911–931 (2019).

[35]M. R. Rashed, M. E. Elsayed, and M. Shaaban, "Influence of magnetically-induced nonlinear added stiffness on the lift galloping of square cylinders at low Reynolds number," J. Fluids Struct. **124**, 104046 (2024).

[36]M. Bolduc, S. Ziada, and P. Lafon, "Flow-excited acoustic resonance of trapped modes of a ducted rectangular cavity," J. Pressure Vessel Technol. **138**, 031303 (2016).

[37]G. Ghirardo and M. R. Bothien, "Quaternion structure of azimuthal instabilities," Phys. Rev. Fluids **3**, 113202 (2018).

26 July 2024 14:04:15

Published under an exclusive license by AIP Publishing